Data-Based Models of the Global Geospace Magnetic Field: Challenges and Prospects of the ISTP Era

Nikolai A. Tsyganenko

Raytheon STX Corp., NASA GSFC, Greenbelt, Maryland

The global magnetic field dominates many of the physical processes of geospace. It is critically important to predict and quantitatively model that field, given information on the state of the incoming solar wind. The ISTP project is an abundant source of data on the distribution and dynamics of the magnetic field and on that field's response to the solar wind variations. Together with earlier sets of spacecraft magnetometer data, the new ISTP data will provide an unprecedented pool of experimental information on the magnetic environment of our planet. Combining this wealth of data with the newest mathematical methods for representing the geomagnetic field will significantly advance our knowledge on the structure and dynamics of the Earth's magnetic environment.

1. INTRODUCTION

The geomagnetic field is one of the most important features of the near-Earth space environment. It links the interplanetary medium (and, hence, the solar atmosphere) with the Earth's ionosphere, guides energetic particles produced by solar activity, channels low-frequency electromagnetic waves and heat flux, confines the radiation belt and auroral plasma, and serves as a giant storehouse of solar wind energy, released during magnetic storms. All these aspects are closely related to the problem of forecasting conditions in the Earth's plasma environment, which is why magnetic field models play a central role in the recent US interagency "space weather" initiative.

A large database of spacecraft magnetometer measurements made by many missions of the last three decades has given us a wealth of information on the structure of Earth's distant magnetosphere and on its response to varying solar wind conditions. This information, however, is often hidden behind chaotic fluctuations, due to the complex nature of the solar-wind-magnetosphere interaction. To reveal the coherent structure underlying the data, one needs flexible mathematical representations for the principal magnetospheric field sources, parametrized by the characteristics of the solar wind and by available geophysical indices. These mathematical "modules", combined into a global model, are then fitted to the entire body of magnetospheric and solar wind data, making it possible to extract information on the global configuration of the geomagnetic field and its response to varying external conditions.

In recent years, significant progress was made in the data-based modeling of the magnetosphere. In contrast to earlier magnetic field representations [*Mead and Fairfield,* 1975; *Tsyganenko,* 1987, 1989], the new-generation models [*Tsyganenko*, 1995, 1996] have a realistic explicitly defined magnetopause, whose size is parametrized by the solar wind pressure, and an IMF-controlled interconnection field across the boundary. Another important new feature is the field from the Region 1 and 2 Birkeland currents [*Tsyganenko and Stern,* 1996]. The amplitude of the field-aligned currents was found from data and parametrized by solar wind characteristics [*Tsyganenko,* 1996].

The purpose of this paper is to give a brief review of the data-based approach, highlight the latest developments, and discuss the new prospects emerging from the availability of the freshly obtained data of the ISTP spacecraft.

Geospace Mass and Energy Flow: Results From the International Solar-Terrestrial Physics Program
Geophysical Monograph 104

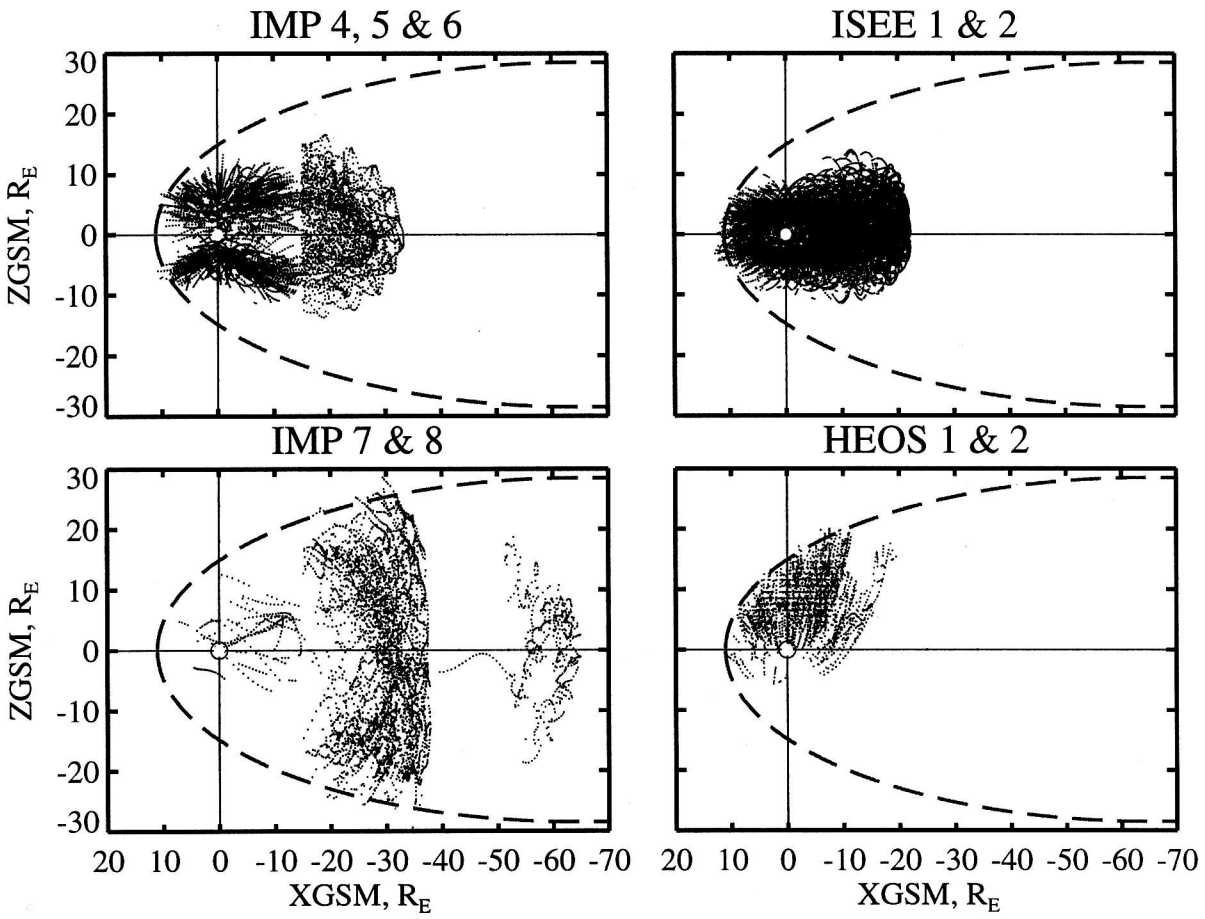

Figure 1. Illustrating the coverage of the magnetosphere by the pre-ISTP spacecraft, which contributed in the currently used data set by *Fairfield et al.* [1994]. The data points are displayed in projection on the noon-midnight meridian plane, and the average position of the magnetopause is shown by broken line.

2. DATA SETS FOR THE MODELING

Over the past three decades, an immense quantity of space magnetometer data has accumulated, collected by many spacecraft at different locations, seasons, and during different solar wind conditions and disturbancy levels. *Mead and Fairfield* [1975] compiled the first set of magnetic field data using four IMP spacecraft during 1966-72, and from that dataset they created an empirical model of the distant field, binned by the Kp-index. *Tsyganenko and Usmanov* [1982] extended the set of Mead and Fairfield by adding HEOS-1 and -2 data and developed a more realistic model with explicitly defined ring current and tail current sheet. Subsequently, the IMP-HEOS set of Tsyganenko and Usmanov was further extended by Tsyganenko and Malkov [see *Peredo et al.*, 1993] by adding ISEE 1/2 data from 1977-81 to the database, while Fairfield independently added HEOS observations along with additional IMP-6 data to the original Mead-Fairfield data base. Additional editing of these data sets and their merging into one large database was done by *Fairfield et al.* [1994], yielding the latest version of the modeling data set, used in the derivation of the new-generation global field model [*Tsyganenko,* 1996].

Each orbital pass contributing to the original high-resolution data was plotted, and a selection of the intervals inside the magnetosphere was made for it. To reduce the very large quantity of data to a manageable size, the values of the field components and of the spacecraft position were averaged, so that consecutive values corresponded to significantly different locations. Finally, the values of the field components were tagged by simultaneous values of the solar wind plasma and magnetic field parameters, compiled by J.H. King at NSSDC [*King,* 1977], as well as by the simultaneous values of the AE/Dst/Kp indices. The total number of the data points in the final set was 79,745, though for a significant part of the data (≈40%) simultaneous solar wind plasma and IMF information was not available. Figures 1a-d show noon-midnight projections of the data point locations for the principal con-

tributors to the database of *Fairfield et al.* [1994]: (a) the IMP-4,-5,-6 spacecraft, (b) ISEE-1 and -2, (c) IMP-7,-8 and Explorer-33,-35, and (d) HEOS-1 and -2 data.

Due to inaccuracies of spacecraft attitude determination, data taken closer than $\sim 4R_E$ were not included in the sets. In general, the coverage is quite non-uniform: the points are relatively dense at middle latitudes in the intermediate range of distances ($5 \leq R \leq 20R_E$), but become much sparser at higher latitudes. At larger distances a spread-out cloud of IMP-7 and -8 data covers the range $25 \leq R \leq 40R_E$, separated by a wide gap from a handful of Explorer-35 data points around the Moon's orbit.

In spite of the incomplete and non-uniform data coverage, the existing set proved to be a valuable source of information on the distant geomagnetic field. It not only allowed average static field configuration to be obtained, but also made it possible to reveal the response of individual magnetospheric current systems to changes in the solar wind, specifically, to its plasma flow pressure and the IMF conditions, as discussed in more detail in the next sections. At first glance, the size of the modeling data set seems quite large; however, considering the enormous spatial extent of the modeling region, gaps in the coverage, and the fact that each global parameter adds another dimension, it becomes clear that more data are urgently needed. To provide the necessary information about all current systems, the data should adequately sample all regions - not only in the (X,Y,Z) space, but also in the added dimensions of the geodipole tilt angle, the geomagnetic activity level (e.g., Dst-index), solar wind presure, and the IMF components.

The new ISTP observations can fill numerous gaps in the existing coverage. Figure 2 shows the distribution of the GEOTAIL positions, projected on the GSM X-Y plane and separated by 1-hour intervals.

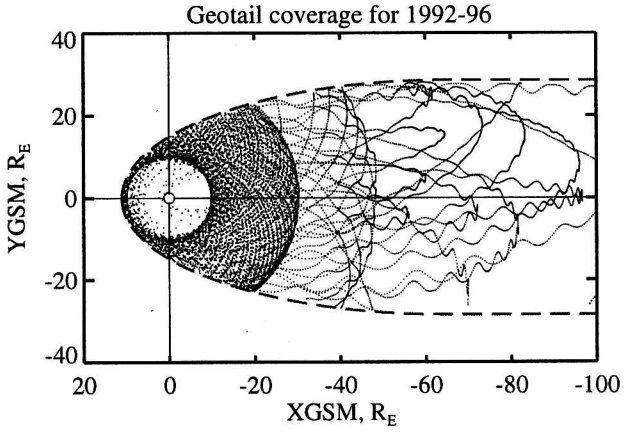

Figure 2. Coverage of the magnetosphere up to tailward distance of $100R_E$ by the Geotail observations. The data points are projected on the GSM equatorial plane.

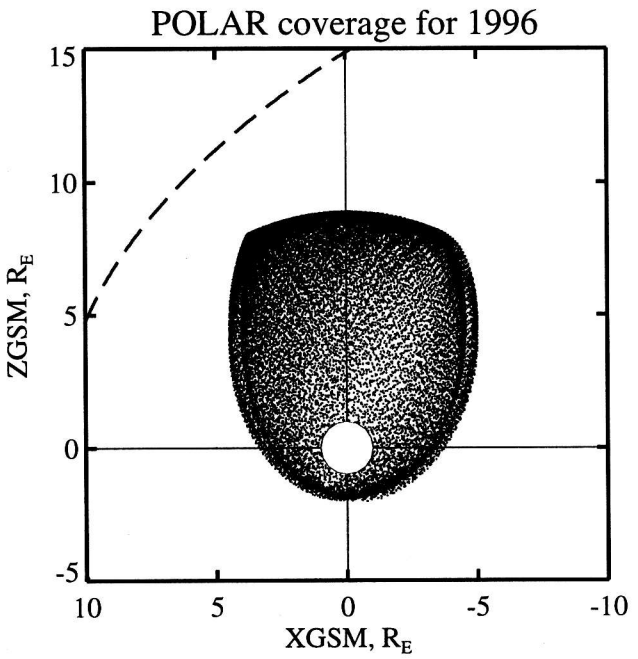

Figure 3. Coverage of the near-Earth magnetosphere by POLAR spacecraft in 1996.

Combined with simultaneous IMP-8 data on the solar wind parameters, the GEOTAIL magnetometer experiment will add to the existing database, as a rough estimate, about 6000 hours worth of data taken inside the magnetosphere.

Inclusion of WIND data (taken both in the solar wind and in the magnetosphere) will further extend the database. An additional advantage of the inclusion of the GEOTAIL data into the modeling data set will be a significant improvement of the equatorial coverage, owing to the relatively low inclination of the GEOTAIL orbit, in comparison with the family of IMP spacecraft.

Another important addition to the existing dataset will be data from POLAR. Due to its highly inclined orbit, that spacecraft will greatly improve the sampling of the high-latitude region, permeated by Birkeland currents. The urgent need for exploring the magnetic field in that region, relevant to the establishing of the large-scale structure of field-aligned currents and to their response to the solar wind parameters, was recognized long ago. The only systematic information on Birkeland currents, so far, has come from low-altitude satellites such as TRIAD and MAGSAT; however, it still remains largely unclear, where field-aligned currents (especially, those of Region 1) come from. Figure 3 displays a distribution of the POLAR positions for 1996, separated by 5-min intervals of time.

Another potential benefit of using the POLAR data can be the development of a more realistic model of the polar cusp region. It has been found in the past [e.g., *Fairfield*, 1991] that the diamagnetism of the polar cusp plasma reveals

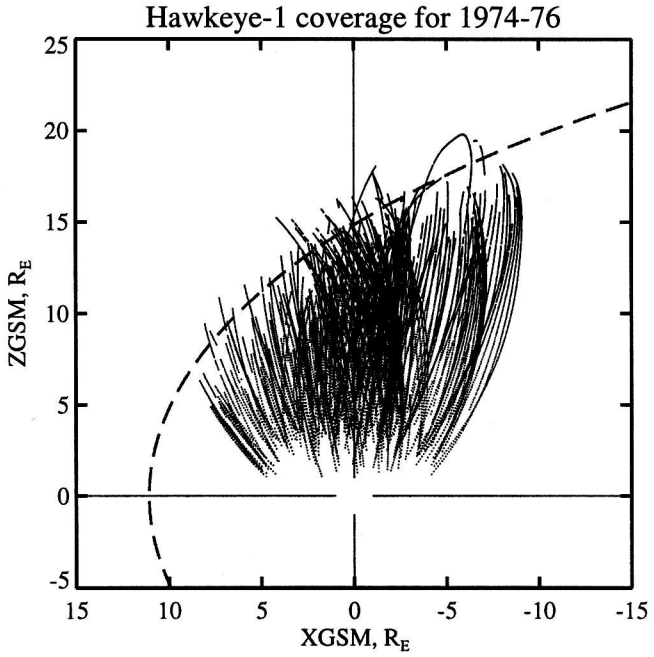

Figure 4. Coverage of the high-latitude magnetosphere by Hawkeye-1 spacecraft in 1974-76.

itself in the deviations of the model magnetic field from that measured inside the polar cusps.

The structure of the polar magnetosphere at higher altitudes was probed in the past by the high-apogee spacecraft HEOS-1, HEOS-2, and Hawkeye-1. The data from the first two were included in the existing database of *Fairfield et al.* [1994] (see Figure 1d above). Figure 4 shows the data cloud for the Hawkeye subset, which is being added to the database.

Another very important domain is the near-Earth equatorial magnetosphere, the region where substorm explosions are believed to be "ignited". New sets of the magnetic field data from that region have been compiled recently. The CRRES data (taken in 1990-91) span a relatively limited range of distances, extending to the spacecraft apogee at $R \approx 6.3R_E$; nevertheless, the dataset is a valuable addition to the modeling data base, since it greatly improves the coverage of the near-equatorial region occupied by the radiation belt. The AMPTE/CCE data set is of unique importance due to the nearly equatorial orbit of the spacecraft, covering a wider range of distances than CRRES, up to the $R \approx 8.8R_E$, and spanning a relatively long period of four years (1984-88). Figure 5 shows the distribution of CRRES and AMPTE/CCE data points. Finally, a huge amount of data on the dynamics of the inner magnetosphere is provided by the extensive set of geosynchronous measurements by GOES satellites, made during 1986-94. Although some of the data contain systematic errors due to magnetic fields generated aboard the spacecraft, most of them are of decent quality and are thus a rich additional resource for magnetospheric field modeling.

3. MODELING THE MAGNETOPAUSE AND DERIVATION OF THE SHIELDING FIELD

The essence of modeling lies in combining the data with flexible mathematical forms, providing a realistic representation of the main individual sources of the total observed field. In devising these forms, we make appropriate assumptions based on the physics (e.g., the magnetopause shielding fields are assumed as curl-free gradients of suitable scalar potentials) and employ all available independent observations (e.g., use a model of the magnetopause based on the direct crossings data).

Knowing the magnetopause position as a function of the upstream solar wind conditions plays a key role in modeling the field configuration inside the magnetosphere. The solar wind confines (shields) the fields produced by all internal sources, by adding to them Chapman-Ferraro field due the current flowing on the magnetopause. In a crude approximation, this results in a "closed" geometry of the total field with $B_n = 0$ on the boundary. Once the position of the magnetopause is known, it is in principle possible to calculate the shielding fields for all internal sources (dipole, ring currentm tail, etc.)

In actuality, B_n is not always zero, which entails important consequences for the physics. The distribution of the normal component B_n on the magnetopause defines the amount of the solar wind magnetic flux linking the geomagnetic field to the solar wind and, hence, the magnitude of the externally induced electric fields in the magnetosphere and ionosphere. That important feature can also be reproduced by the data-based models.

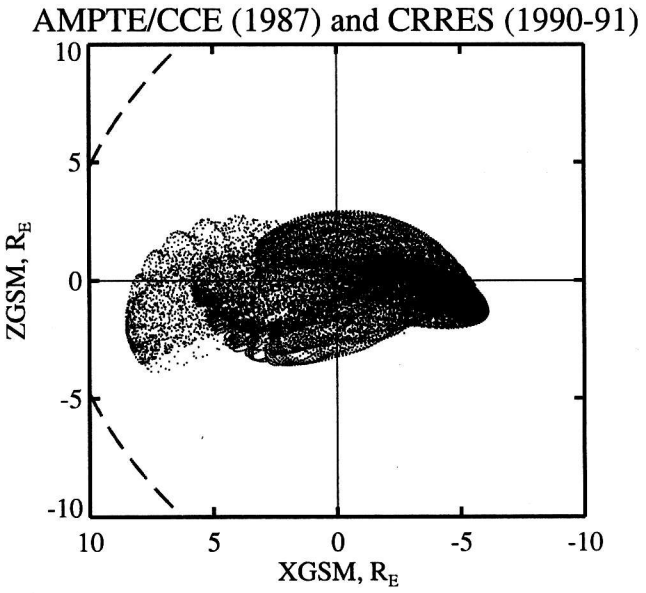

Figure 5. Coverage of the near-Earth equatorial magnetosphere by AMPTE/CCE and CRRES spacecraft.

In the deriving the earlier models [*Mead and Fairfield,* 1975; *Tsyganenko and Usmanov,* 1982; *Tsyganenko,* 1987, 1989] no direct information about the shape and position of the magnetopause was used. Neither did those models specify that shape and position explicitly. Instead, the magnetopause appeared as a "de-facto" surface that separated two families of field lines: those with no connection to Earth and those crossing Earth's surface at least once. In essence, this "de-facto" magnetopause represented an outward extrapolation of the model field beyond the region covered by measurements. On the dayside, its shape and size did not differ much from those observed. However, because of the poorer coverage of the high-latitude tail lobes, at larger distances the shape of the field lines became unstable and resulted in unrealistic features of the "de-facto" boundary.

This motivated us to look for a more rigorous mathematical treatment of the magnetopause and its shielding field. Significant progress in this area was made recently, based on two cornerstones, discussed below in more detail. The first one is the empirical modeling of the magnetopause shape and size using data of actual boundary crossings [*Sibeck et al.,* 1991; *Roelof and Sibeck,* 1993], and the second is an approximate method for the derivation of the shielding field for a wide class of general boundaries, using the least squares minimization of magnetic flux across the magnetopause [*Schulz and McNab,* 1987, 1996].

The first empirical models of the magnetopause shape, based on spacecraft crossing observations were developed by *Fairfield* [1971], *Howe and Binsack* [1972], and *Formisano et al.* [1979]. *Sibeck et al.* [1991] further developed that approach by extending the database of boundary crossings and *Roelof and Sibeck* [1993] introduced a bi-variate parameterization of the model boundary by both the solar wind ram pressure and IMF B_z.

In the latest version of the data-based magnetospheric field model [*Tsyganenko,* 1996] the magnetopause model of *Sibeck et al.* [1991] was adopted for the front of the boundary ($X_{GSM} > -50R_E$) and was then smoothly extended tailward as a cylinder with the radius $R \approx 28R_E$. No IMF dependence of the magnetopause shape and size was assumed in that model, while the effects of pressure variations were simulated by a self-similar compression/expansion. The scaling factor κ was assumed as $\kappa = (p/p')^{\alpha}$, where the index α was a free model parameter. Its best-fit value $\alpha \approx 0.14$ was found to be quite close to $\alpha = 1/6$, given by simple theory [e.g., *Mead and Beard,* 1964].

The assumption of self-similar scaling of magnetopause dimensions by $\kappa(p)$ greatly simplifies the task of maintaining the shielding condition (or, more generally, keeping B_n on the boundary under control) for different pressure values, since in that case re-calculation of the shielding field can be reduced to a simple scaling. However, as shown by *Roelof and Sibeck* [1993], self-similarity should only be considered as a rather crude approximation: in the limit of strong

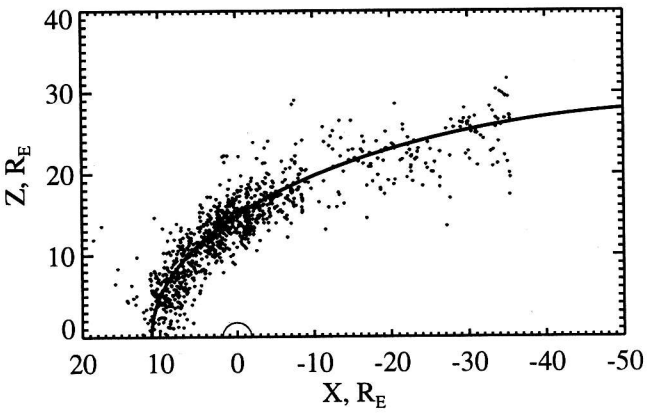

Figure 6. The shape of the model magnetopause for average solar wind conditions and the positions of the observed boundary crossings, rotated into the $X - Z$ plane.

northward and southward IMF B_z, the response of the magnetopause shape to variations of the pressure is substantially different from a self-similar change in size. The IMF-related change of the boundary shape does not seem to modify the internal field structure in any major way; however, it becomes important in the evaluation of the IMF interconnection with the geomagnetic field across the magnetopause, as will be discussed below in more detail.

Figure 6 shows the shape of the model magnetopause for average solar wind conditions, adopted in the data-based model by *Tsyganenko* [1996], and the cloud of boundary crossing points, compiled from the set of *Sibeck et al.* [1991] and further extended by adding crossings by Hawkeye-1 during 1974-75 [*Tsyganenko et al.,* 1996].

Once the analytically prescribed boundary is available, it is possible to derive a shielding field for any internal electric current system, by specifying a set of suitable curl-free fields with a sufficient degree of flexibility and combining those fields by least squares fitting, to make the resultant B_n on the boundary as close as possible to its desired distribution. *Schulz and McNab* [1987] were first to implement that idea in developing their "source-surface" model of the magnetosphere. Subsequently, the method was extended for the derivation of shielding fields for all principal sources of the magnetospheric magnetic field in data-based models, including the ring current and the tail current sheet [*Tsyganenko,* 1995] and the Region 1/2 Birkeland currents [*Tsyganenko and Stern,* 1996]. With a slight modification, the same method can be used for the derivation of the IMF interconnection field inside the magnetosphere, based on a prescribed distribution of B_n on the boundary [*Tsyganenko,* 1996].

As an example, Figure 7 displays a configuration of the magnetic field produced by a model ring current, confined inside the model magnetopause. In this case, the shielding field $\vec{\mathbf{B}}_{sh} = -\nabla U$ was represented by a sum of 8 cylindrical harmonics and included a dependence on the geodipole tilt angle Ψ

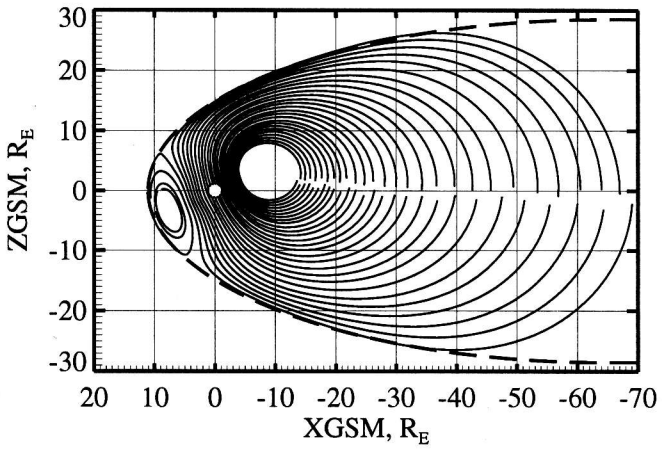

Figure 7. Lines of the magnetic field produced by the model ring current, fully confined within the model magnetopause by the shielding field (1). The north-south asymmetry is due to the tilt of the Earth's dipole, which affects the position of the ring current.

$$U = \cos\Psi \sum_{i=1}^{2} \sum_{m=1,3} a_{im} J_m(\rho/p_{im}) \exp(x/p_{im}) \sin m\phi$$

$$+ \sin\Psi \sum_{i=1}^{2} \sum_{m=0,2} b_{im} J_m(\rho/q_{im}) \exp(x/q_{im}) \cos m\phi \qquad (1)$$

The coefficients $\{a_{im}, b_{im}\}$ and nonlinear parameters $\{p_{im}, q_{im}\}$ were found by an iterative algorithm, combining a standard linear least-squares fitting of $\{a_{im}, b_{im}\}$ with a simplex search for the optimal nonlinear parameters $\{p_{im}, q_{im}\}$ [*Press et al.*, 1992].

All other internal sources can be shielded in a similar way; the difference is in the number of terms necessary for satisfying the boundary conditions with sufficient accuracy. The tail current sheet and the Region 1 system of Birkeland currents require more terms in (1), because they extend to larger distances and create a strongly non-uniform field near the magnetopause.

The primary reason for explicitly including the shielding fields in the models is to control the degree of interconnection between the field of terrestrial origin and the IMF. Most of the recent progress in this area was made possible by the "modular approach", in which separate internal sources of the magnetospheric field were modeled by separate terms with their own amplitude coefficients, parameterized by appropriate combinations of solar wind characteristics [Tsyganenko, 1996]:

$$\mathbf{B} = \mathbf{B}_{Earth} + \mathbf{B}_{Tail} + \mathbf{B}_{RC} + \mathbf{B}_{Birk} + \mathbf{B}_{int} \qquad (2)$$

The consecutive terms on the righthand side denote, respectively, the contributions from the Earth's main field, the tail current sheet, the ring current, Birkeland currents, and the interconnection term, representing the effect of non-zero B_n and IMF penetration. It is implicitly assumed in (2) that each term on the right-hand side, except for the last one, includes its own "partial" magnetopause field, so that the net field from internal magnetospheric sources remains fully shielded inside the boundary, for any combination of amplitudes of the individual terms.

The last term in (2) represents the effect of the IMF penetration. Due to the full shielding of other terms, the corresponding normal component of the total field on the boundary is reduced to $B_n = (\mathbf{B}_{int} \cdot \mathbf{n})$, where the vector $\mathbf{B}_{int}$ was assumed to be proportional to the transverse component of the IMF $\vec{\mathbf{B}}_t = B_y\vec{\mathbf{e}}_y + B_z\vec{\mathbf{e}}_z$. The proportionality factor was determined from data.

Fitting several versions of the above model field to the data, tagged by the solar wind parameters, yielded persistently large values of the proportionality factor (~0.8) [*Tsyganenko,* 1996]. It was also found that the penetration efficiency was almost independent of the direction of the transverse component of the IMF, that is, the penetration pattern just rotated around the Sun-Earth line, as if rigidly tied to that component.

More recent studies recognized, however, that a subtle effect must be taken into account here, or else a systematic overestimate of the penetration field may arise. So far, all derivations of $\mathbf{B}_{int}$ were based solely on magnetic field vectors observed inside the magnetosphere, many of them in the magnetotail. But the boundary of the tail, especially near Earth, spreads outwards – its diameter increases with distance from Earth. Lobe field lines, especially those far from the plasma sheet, tend to follow the boundary and therefore also diverge outwards, an effect which gives them a southward B_z, increasing when the flaring angle of the boundary grows larger.

On the other hand, one should expect that the magnetopause flaring angle also increases during times of southward IMF, due to an increased reconnection rate. If a larger southward B_z is then observed inside the tail, it is hard to tell offhand what part of it is caused by the added penetration of the IMF and what part by greater flaring of the boundary.

This ambiguity cannot be resolved by models, in which the solar wind effects upon the magnetopause are reduced to the pressure-controlled expansion and compression, with no dependence of the boundary shape upon the IMF. On the other hand, introducing a magnetopause model with a bivariate dependence of shape and size, similar to that of *Roelof and Sibeck* [1993], meets with two problems. The first one is the above mentioned need to recalculate the shielding field parameters for any new combination of the solar wind parameters, since the corresponding changes in the boundary shape are no longer self-similar. The second problem is a sparsity of magnetopause crossing data tailward of $x \sim -10R_E$ and the almost total absence of such data in the middle and far tail, which limits the reliability of magnetopause models in that region and, hence, makes it difficult to separate the effects of the tail flaring from those of the IMF penetration.

Observations of magnetopause crossings by the ISTP spacecraft (GEOTAIL, IMP-8, and WIND), made during recent years, will provide a valuable addition to the existing dataset and may help in obtaining more reliable estimates of the reconnection of the interplanetary magnetic flux. Combining that data with models of the magnetosheath plasma flow [e.g., *Spreiter and Stahara,* 1980] can allow us to derive the expected distribution of the solar-wind-induced electric field in the polar caps in a way similar to what was done by *Toffoletto and Hill* [1989, 1993]. The resulting electric potential pattern can then be compared to the one given by independent data-based models of the ionospheric convection [e.g., *Heppner and Maynard,* 1987].

4. MODELING THE RING CURRENT AND THE TAIL CURRENT SYSTEM

There exist several known methods to analytically represent the field produced by the ring current. *Tsyganenko and Usmanov* [1982] suggested a model, based on a simple mathematical modification of the vector potential of a dipole. It is probably the simplest possible model with only two parameters: the ring current amplitude and its characteristic radius. The principal deficiency of the model stems from its extreme simplicity: the electric current is excessively spread out in space, and there is no easy way to control its distribution. *Hilmer and Voigt* [1995] used a combination of two models of that kind with different scale sizes for modeling a more realistic ring current, including a zone of eastward $\vec{\mathbf{j}}$ at the inner boundary of the radiation belt.

Tsyganenko and Peredo [1994] suggested a more flexible model, based on a superposition of analytical vector potentials for current disks with a controllable finite thickness. The radial distribution of the current density in that kind of model can be adjusted by an appropriate choice of the expansion coefficients and by scaling the field as a whole. That type of the ring current was used in the new global models, parameterized by the solar wind pressure, IMF, and Dst-index [*Tsyganenko,* 1995; 1996].

Here we describe another model, combining flexibility and realism with a very fast computational performance. The basic idea is to start from the vector potential for a circular current loop [e.g., *Smythe,* 1950]:

$$\vec{\mathbf{A}} = \frac{(1 - k^2/2)K(k) - E(k)}{k\rho^{1/2}}\vec{\mathbf{e}}_\phi , \qquad (3)$$

where $E(k)$ and $K(k)$ are complete elliptical integrals of the 1st and 2nd kind, and modify the original form of the function $k(\rho, z)$ by adding a term D^2 in the denominator, so that

$$k^2 = \frac{4R\rho}{(R+\rho)^2 + z^2 + D^2} \qquad (4)$$

This results in a spreading out of the originally infinitely thin current loop over all of space. However, most of the current remains localized in the vicinity of the loop, so that the current density peaks at $\rho = R$, $z = 0$, and rapidly falls off to zero with increasing distance from the loop. The variable D specifies a characteristic thickness of the current, and can be made a function of position without violating the condition $\nabla \cdot \vec{\mathbf{B}} = \mathbf{0}$. In particular, taking $D = D(x)$ makes it possible to model the day-night asymmetry of the ring current (or the dawn-dusk asymmetry, with $D = D(y)$). Combining two distributions with different characteristic radii R allows a realistic ring current to be modeled, reversing to an eastward directed current in the inner magnetosphere, an effect of the pressure gradient. Figure 8 illustrates an example of such a model ring current, displaying radial profiles of the magnetic field disturbance (left panel) and the volume current density (right panel).

The tail current system has been recently modeled by using the above described approach with analytical spread-out current disks [*Tsyganenko and Peredo,* 1994; *Tsyganenko,* 1995]. To achieve a greater flexibility in modeling the extended current sheet on the nightside, the tail field was represented as a combination of several modes having different tailward variation scale distances and different weight amplitudes, with those parameters determined from fitting the model to data.

The analytical disk-like modes have an inconvenient feature: for large radial distances r, individual terms in the corresponding expansions for the tail field decrease as r^{-2}, while the actual far-tail lobe B varies more slowly [e.g., *Slavin et al.,* 1985]. By combining several terms, it is in principle possible to obtain a slower decrease over a limited range of X_{GSM} with a sufficiently steep inner edge of the current sheet. However, the number of terms necessary for maintaining a realistic profile becomes too large when one tries to extend the tail model to larger distances. For that reason, in the last release of the model [*Tsyganenko,* 1996] a disk-like mode was combined with an "asymptotic" mode, based on another model of the current sheet, suggested in our earlier work [*Tsyganenko,* 1987], in which the current flows along straight lines in the Y-direction, and its density in the limit $x \to -\infty$ tends to a finite value, rather than to zero. That term provided a smooth transition from the rapidly varying field in the near tail to the almost uniform $\mathbf{B}$ in the far tail, where the actual lobe field is nearly constant. Even with just a few hundred data points in the far tail, contributed by the Explorer-35 magnetometer, this approximation yielded quite realistic values of the best-fit quiet-time asymptotic magnetotail field B_∞ and of the coefficient defining its response to changes in the solar wind pressure around its average value P_0:

$$B_\infty = 6.7 + 5.5\left(\sqrt{P/P_0} - 1\right) \qquad (5)$$

This result suggests that adding new data of GEOTAIL to the

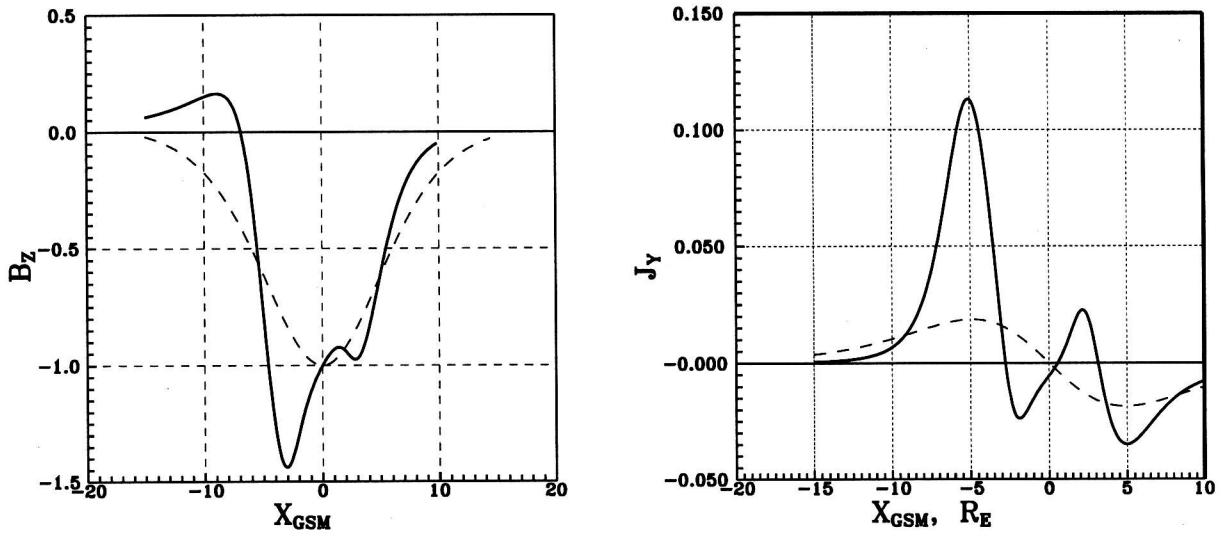

Figure 8. Variation along the Sun-Earth line of the B_z component of the magnetic field (left) and the corresponding profile of the azimuthal electric current density (right) in the model ring current. Both quantities are plotted in arbitrary units.

already available data will extend the model to more distant regions.

5. INCLUSION OF BIRKELAND CURRENTS IN THE MODEL

One of the most recent breakthroughs in the data-based modeling of the magnetospheric field was the inclusion of the global field of the Region 1 and 2 field-aligned currents [*Tsyganenko and Stern,* 1996]. Long before that, the great role played by the Region 1 currents in the magnetic structure of the outer dayside magnetosphere was realized [e.g., *Maltsev and Lyatsky,* 1975; *Tsyganenko and Usmanov,* 1984]. The latest results, discussed in the next section, give more evidence for the strong effect of the global system of Region 1 Birkeland currents upon the position of the polar cusps.

A principal difficulty with Birkeland currents, not found in other current systems, is the lack of information on their actual global configuration. Little is as yet known on how far from Earth do the Birkeland currents remain field-aligned and on where they close. Existing observations [*Iijima and Potemra,* 1976; *Tsyganenko et al.,* 1994] and recent results of MHD simulations [*Tanaka,* 1995; *Janhunen,* 1996] suggest two important features: first, that Region 1 currents strongly depend on the IMF orientation both in their magnitude and geometry and, second, that most of them flow in the dayside and dawn-dusk magnetosphere, at least for southward IMF conditions.

The new model of the field-aligned current systems [*Tsyganenko and Stern,* 1996] is based on an Euler potential representation for the current density and on existing data on the geometry and distribution of Birkeland currents at ionospheric altitudes and at larger distances. The variation of the current strength along the ionospheric Region 1 and 2 ovals was specified to fit the statistical results of *Iijima and Potemra* [1976]. The parameters to be found from data were the coefficients relating the total current in both systems with the solar wind pressure and IMF. The principal results of the data-based modeling about field-aligned currents will be briefly discussed in the next section.

However, modeling the Birkeland currents is still in its infancy, and much remains to be done. The most important limitation of the existing model is the assumption of a fixed geometry of the current, regardless to IMF conditions. In future upgrades of the magnetospheric models, more flexibility will be allowed for the field-aligned current by splitting the term $\mathbf{B}_{Birk}$ into a sum of independent modes with variable IMF-dependent coefficients. As already mentioned, a substantial input is expected from the POLAR data, since they cover a relatively unexplored region and can provide a valuable information on field-aligned currents at intermediate distances.

6. SOLAR WIND EFFECTS IN GLOBAL MODEL FIELD CONFIGURATIONS

The optimal way of extracting from the data information on the solar wind control of individual current systems would be to specify an analytical dependence of the model field on all input variables (e.g., solar wind pressure, IMF components, and Dst) and then fit the model to the entire set of data. A simpler method, used in the earlier models, was to divide the data into several subsets, each covering a different interval of the model input parameter (e.g., Kp-index) and then to

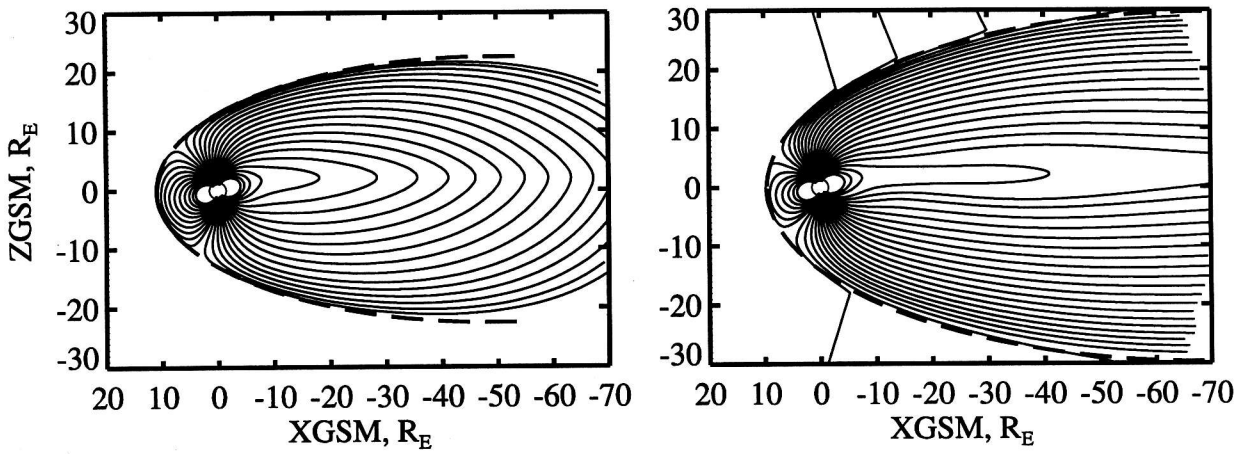

Figure 9. Configurations of the model magnetic field lines for opposite polarities of the IMF B_z-component: $B_z > +5nT$ (left) and $B_z < -5nT$ (right). In both cases, the same values were used for the solar wind pressure and the Dst-index. Note a striking difference in the amount of the magnetic flux both on the day and night sides.

separately fit the model to the subsets, generating separate sets of coefficients. However, with a larger number of input parameters, this approach becomes unfeasible due to rapidly growing number of bins in the multi-dimensional parameter space, leaving too few data points in each of the individual subsets.

In the last version of the global model [*Tsyganenko,* 1996], the input solar wind parameters and the Dst-index entered the field components as continuous variables and were therefore treated in the same way as the spatial coordinates $\{x, y, z\}$ and the geodipole tilt angle Ψ. That approach avoided the binning of the database into smaller sets and, hence, allowed more effective extraction of the information contained in the data. However, the price of this was sacrificing the ability of the model magnetopause to change its shape in response to changes of the IMF polarity. It was assumed that the only parameter controlling the size of the boundary was the solar wind pressure, which allowed fast recalculation of the shielding field, as already discussed in Section 3.

In this section, we discuss the results of the most recent global modeling study on the response of the magnetospheric field structure to changes in the solar wind state, for two opposite extremes of the polarity of the north-south component of the IMF [*Tsyganenko et al.,* 1996]. It was aimed at a more accurate estimate of the IMF interconnection effect, taking into account the IMF-induced changes of the magnetopause shape. For that reason, instead of a continuous parameterization by the IMF B_y and B_z, we had to retreat to the old binning approach with regard to the IMF, having retained a continuous dependence on the wind pressure.

Two subsets were compiled from the entire modeling database, including the data taken during periods with strongly northward and strongly southward IMF. More specifically, the first subset contained the data points with IMF $B_z > +5nT$, and the second one with $B_z < -5nT$. In both cases, an additional constraint $B_y < 5nT$ was imposed on the azimuthal IMF component, to make sure that effects of the north-south component were predominant. The numbers of data points in the two subsets were 1787 and 1722, respectively.

The next step was to construct pressure-driven magnetopause models for the two opposite IMF polarities. For simplicity, effects of the IMF and of the pressure p upon the boundary position were reduced to two fundamental separate modes: (i) a self-similar compression/expansion, driven by p, and (ii) an IMF-driven change of the shape of the boundary, in which an earthward shift of the dayside magnetopause was accompanied by an increase of the tail radius. The individual response amplitudes of the two modes were represented as simple functions of p and IMF B_z, evaluated by least squares fitting of the model boundary to the data set of the magnetopause crossings, in the same way as was done by *Roelof and Sibeck* [1993].

Using the two magnetospheric data subsets and magnetopause models, two sets of model coefficients were found by least squares, for IMF $B_z > +5nT$ and for IMF $B_z < -5nT$.

Figure 9 shows two configurations of the field lines in the noon-midnight meridian plane, for the same values of $p = 4nPa$ and Dst=0, but for opposite IMF polarities: $B_z > +5nT$ (left panel) and $B_z < -5nT$ (right panel).

As seen in the plots, there is a striking difference between the two configurations. First, changing the IMF from strongly northward to southward decreases the polar cusp footpoint latitude from $\sim 80°$ to $\sim 71°$. This shift is primarily due to the large increase of the total strength of the Region 1 Birkeland current, from nearly zero for northward IMF conditions to $\approx$ 2.4MA for southward IMF. Second, a huge difference can be seen in the amount of the magnetic flux closure across

the tail plasma sheet. This is mostly due to a dramatic redistribution of the tail current: the reversal to strongly northward IMF B_z is accompanied by a nearly complete disappearance of the far-tail current, while, at the same time, no significant change in the amplitude of the near-tail current was found. An additional contribution to this effect comes from the direct penetration of the IMF; however, the overall magnitude of the penetrating field was found to be much smaller than in the model with the IMF-independent magnetopause shape [*Tsyganenko,* 1996]. More specifically, for the strongly northward IMF, the penetrating field was virtually absent, while for strongly southward field, a penetration coefficient of only ≈ 0.17 was obtained.

This finding differs significantly from the strong penetration (≈ 0.8) reported previously [*Tsyganenko,* 1996]. The difference is due to the inclusion of the effects of the IMF-dependent magnetopause, discussed in more detail in Section 3, and the strong correlation of the far-tail current with the IMF (no IMF-dependence of that current was assumed in the earlier model; see Equation 5 above).

The above results demonstrate that even with sparse data subsets and relatively crude time resolution, the data-based models can reproduce the expected global re-configuration of the magnetic field surprisingly well. At the same time, separating the subtle interconnection effects from the background of stronger variations is still a hard task with much uncertainty involved. Adding new data from the ISTP spacecraft and a re-creation of the older datasets with a higher time resolution will increase the reliability of the modeling.

7. MODELING OF THE NEAR-EARTH MAGNETIC FIELD

Many studies require an accurate model of the geophysical environment only within a limited region of the near-Earth space. In particular, the low-latitude region inside $R \approx 10R_E$ is of special importance. From the viewpoint of physics, that is where the most dramatic events of particle injection and of magnetic field re-configuration take place during storms and substorms. In addition, studies of "space weather" effects on communication satellites need reliable, compact, and fast models of the magnetic field in the vicinity of geostationary orbit [e.g., *Rufenach et al.,* 1992].

In some aspects, the local modeling of the near-Earth magnetic field is easier than its global representation. First, the data coverage of this region is relatively dense, accumulated over many years under different solar activity conditions, including a large database of GOES measurements. Second, due to the smaller spatial extent, local models can be made mathematically simpler and hence much faster for computations: for example, the magnetopause field can be represented by simple linear or quadratic expansions. Also, a simpler model for the field of Birkeland currents can be envisioned, because the behavior of the field components at large distances is no longer important. On the other hand, as one descends to smaller spatial scales and shorter time intervals, one can include here effects not covered by global models, for instance, large-amplitude effects of the substorm currents. Attempts were made in the past to model the substorm growth and recovery phases by a modification of the global tail current system [e.g., *Pulkkinen et al., 1994* and references therein]. However, a truly realistic and full description of the substorm disturbance field should include a feasible 3-D model of the current wedge on the nightside. First successful steps in this direction have been made recently [*Tsyganenko,* 1997].

On the dayside, even the existing global models, based on data with relatively crude time resolution, track the field observed at the geosynchronous orbit surprisingly accurately [*Lu et al.*, 1997]. As an example, Figure 10 compares the components of the magnetic field measured there by GOES-5 with those computed using the global model [*Tsyganenko*, 1996]. The best agreement is observed for the B_z-component: in this example and in many other cases we found an almost perfect match between the model and the data in the pre-noon sector. Note that even short-scale excursions of B_z are reproduced with remarkable accuracy. A closer inspection showed that those excursions were due mainly to variations in the IMF B_z, which controls the intensity of the model Birkeland currents and also contributes through the term for the directly penetrating IMF.

Another important feature, still awaiting its proper representation in models, is the dawn-dusk asymmetry of the storm-time equatorial field, conspicuous at geosynchronous distance [*Coleman and McPherron,* 1976]. ISTP data, first of all those of POLAR and GOES, will significantly improve the coverage of high- and low-latitude regions of the inner magnetospphere and will thus promote rapid progress in modeling the near-Earth magnetic environment.

8. SUMMARY

Global data-based modeling of the geomagnetosphere have seen significant progress during the last years. A large arsenal of mathematical methods has been developed recently for modeling all principal sources of the magnetic field. Realistic representations have been devised for the magnetopause, based on direct crossings data and dependent on solar wind parameters. Powerful methods were developed for the derivation of the magnetopause magnetic field, with an IMF-controlled interconnection of terrestrial and solar-wind magnetic fields across the boundary. Large sets of space magnetometer data for modeling have been compiled from the archived higher-resolution data.

A synthesis of the above elements has made it possible to create new-generation models, parameterized by solar wind characteristics and the Dst-index. In spite of a still incom-

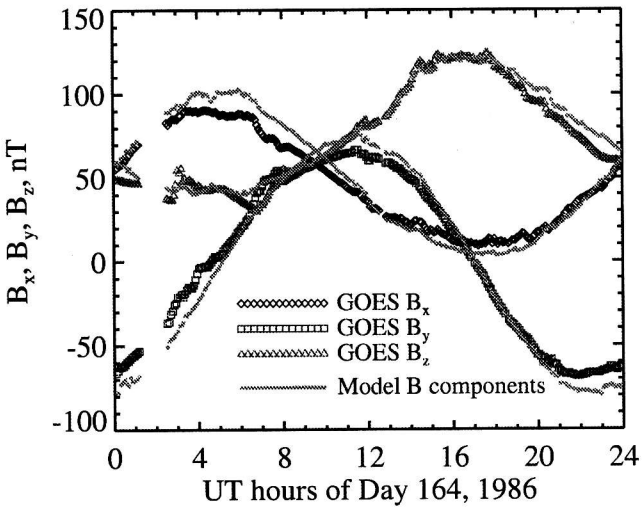

Figure 10. An example of comparison of the diurnal variation of the magnetic field components measured by geosynchronous spacecraft and those obtained from the data-based model.

plete coverage by data, these models reproduce the observed response of the magnetosphere to solar wind input surprisingly well. The newly obtained ISTP data will provide an abundant influx of fresh experimental information. Combining that data with the existing datasets and application of the newest methods will boost our progress in understanding the physical links between the state of the interplanetary medium and the near-Earth magnetic environment.

Acknowledgments. The author is grateful to David Stern for his numerous helpful comments on the manuscript. This work is supported by NASA grants NAS5-32350 and NSF Magnetospheric Physics Program grant ATM-9501463.

REFERENCES

Coleman, P.J. and R.L. McPherron, Substorm observations of magnetic perturbations and ULF waves at synchronous orbit by ATS-1 and ATS-6, in: *The Scientific Satellite Programme During the International Magnetospheric Study*, ed. K. Knott and B. Battrick, p.345, D.Reidel, Dordrecht, 1976.

Fairfield, D.H., An evaluation of the Tsyganenko magnetic field model, *J. Geophys. Res., 96,* 1481, 1991.

Fairfield, D.H., N.A. Tsyganenko, A.V. Usmanov, and M.V. Malkov, A large magnetosphere magnetic field database, *J. Geophys. Res., 99,* 11319, 1994.

Heppner, J.P. and N.C. Maynard, Empirical high-latitude electric field models, *J. Geophys. Res., 92,* 4467, 1987.

Hilmer, R.V. and G.-H. Voigt, A magnetospheric magnetic field model with flexible current systems driven by independent physical parameters, *J. Geophys. Res., 100,* 5613, 1995.

Iijima, T. and T.A. Potemra, The amplitude distribution of field-aligned currents at northern high latitudes observed by Triad, *J. Geophys. Res., 81,* 2165, 1976.

Janhunen, P., H.E.J. Koskinen, and T.I. Pulkkinen, A new global ionosphere-magnetosphere coupling simulation utilizing locally varying time step, in *Proceedings of the ICS-3 Conference on Substorms* (Versailles, France, May 12-17, 1996), ESA SP-389, pp.205-210, 1996.

King, J.H., *Interplanetary medium data book,* NSSDC/WDC-A-R&S 77-04, Natl.Space Data Cent., Greenbelt, MD., 1977.

Lu, G., G.L. Siscoe, A.D. Richmond, T.I. Pulkkinen, N.A. Tsyganenko, H.J. Singer, and B.A. Emery, Mapping of the ionospheric field-aligned currents to the equatorial magnetosphere, *J. Geophys. Res., 102,* 14467, 1997.

Maltsev, Yu.P. and W.B. Lyatsky, Field aligned currents and erosion of the dayside magnetosphere, *Planet.Space Sci., 23,* 1257, 1975.

Mead, G.D. and D.B. Beard, Shape of the geomagnetic field solar wind boundary, *J. Geophys. Res., 69,* 1169, 1964.

Mead, G.D. and D.H. Fairfield, A quantitative magnetospheric model derived from spacecraft magnetometer data, *J. Geophys. Res., 80,* 523, 1975.

Peredo, M., D.P. Stern, and N.A. Tsyganenko, Are existing magnetospheric models excessively stretched ?, *J. Geophys. Res., 98,* 15343, 1993.

Pulkkinen, T.I., D.N. Baker, P.K. Toivanen, R.J. Pellinen, R.H.W. Friedel, and A. Korth, Magnetospheric field and current distributions during the substorm recovery phase, *J. Geophys. Res., 99,* 10955, 1994.

Roelof, E.C., and D.G. Sibeck, Magnetopause shape as a bivariate function of the interplanetary magnetic field B_z and solar wind dynamic pressure, *J. Geophys. Res., 98,* 21421, 1993.

Rufenach, C.L., R.L. McPherron, and J. Schaper, The quiet geomagnetic field at geosynchronous orbit and its dependence on solar wind dynamic pressure, *J. Geophys. Res., 97,* 25, 1992.

Schulz, M., and M. McNab, Source-surface model of the magnetosphere, *Geophys. Res. Lett., 14,* 182, 1987.

Schulz, M., and M. McNab, Source-surface modeling of planetary magnetospheres, *J. Geophys. Res., 101,* 5095, 1996.

Sibeck, D.G., R.E. Lopez, and E.C. Roelof, Solar wind control of the magnetopause shape, location, and motion, *J. Geophys. Res., 96,* 5489, 1991.

Slavin, J.A., E.J. Smith, D.G. Sibeck, D.N. Baker, R.D. Zwickl, and S.-I. Akasofu, An ISEE 3 study of average and substorm conditions in the distant magnetotail, *J. Geophys. Res., 90,* 10875, 1991.

Smythe, W.R., *Static and dynamic electricity,* New York: McGraw-Hill, 1950.

Spreiter, J.R. and S.S. Stahara, A new predictive model for determining solar wind–terrestrial planet interactions, *J. Geophys. Res., 85,* 6769, 1980.

Tanaka, T., Generation mechanisms for magnetosphere-ionosphere current systems deduced from a three-dimensional MHD simulation of the solar wind-magnetosphere-ionosphere coupling processes, *J. Geophys. Res., 100,* 12057, 1995.

Toffoletto, F.R. and T.W. Hill, Mapping of the solar wind electric field to the Earth's polar caps, *J. Geophys. Res., 94,* 329, 1989.

Toffoletto, F.R. and T.W. Hill, A nonsingular model of the open magnetosphere, *J. Geophys. Res., 98,* 1339, 1993.

Tsyganenko, N.A. and A.V. Usmanov, Determination of the magnetospheric current system parameters and development of experimental geomagnetic field models based on data from IMP and HEOS satellites, *Planet. Space Sci., 30,* 985, 1982.

Tsyganenko, N.A. and A.V. Usmanov, Effects of field-aligned currents in structure and location of polar cusps, *Planet. Space Sci., 32,* 97, 1984.

Tsyganenko, N.A., A magnetospheric magnetic field model with the warped tail current sheet, *Planet. Space Sci., 37,* 5, 1989.

Tsyganenko, N.A., D.P. Stern, and Z. Kaymaz, Birkeland currents in the plasma sheet, *J. Geophys. Res., 98,* 19455, 1993.

Tsyganenko, N.A., and M. Peredo, Analytical models of the magnetic field of disk-shaped current sheets, *J. Geophys. Res., 99,* 199, 1994.

Tsyganenko, N.A. Modeling the Earth's magnetospheric magnetic field confined within a realistic magnetopause, *J. Geophys. Res., 100,* 5599, 1995.

Tsyganenko, N.A. and D.P. Stern, Modeling the global magnetic field of the large-scale Birkeland current systems, *J. Geophys. Res., 101,* 27187, 1996.

Tsyganenko, N.A., Effects of the solar wind conditions on the global magnetospheric configuration as deduced from data-based field models, in *Proceedings of the ICS-3 Conference on substorms* (Versailles, France, May 12-17, 1996), ESA SP-389, pp.181-185, 1996.

Tsyganenko, N.A., M. Peredo, S. Boardsen, and T.E. Eastman, Interconnection of IMF with the geomagnetic field: What can data based models tell us ?, *Eos Trans. AGU, 77,*(46), Fall Meet.Suppl., F638, 1996.

Tsyganenko, N.A., An empirical model of the substorm current wedge, *J. Geophys. Res., 102,* 19935, 1997.

N. A. Tsyganenko, Raytheon STX Corporation, Laboratory for Extraterrestrial Physics, Code 690.2, NASA Goddard Space Flight Center, Greenbelt, MD 20771. (e-mail: kolya@nssdca.gsfc.nasa.gov)